Journal of Materials Science and Chemical Engineering, 2026, 14(8), 30-57
https://www.scirp.org/journal/msce
ISSN Online: 2327-6053
ISSN Print: 2327-6045

Assessing the Suitability of Zimado Clay as a Precursor for Sustainable Lightweight Expanded Clay Aggregate (LECA) Production

Abraham Zigla Atour[1*], Darman Japhet Taypondou[1], Hippolyte Todou Assaouka[2], Pieride Mabe Fogang[1], Vincent de Paul Zoua[3], Patrick Mountapmbeme Kouotou[4], Etienne Yanné[5]

[1]Department of Civil Engineering, National Advanced School of Public Works, Yaoundé, Cameroon
[2]Department of Chemistry, Faculty of Science, University of Garoua, Garoua, Cameroon
[3]Department of Fundamental and Cross-Cutting Sciences, National Advanced School of Public Works, Yaoundé, Cameroon
[4]Research, Experimental and Production Centre, Higher Institute of Agriculture, Wood, Water and Environment, University of Ebolowa, Ebolowa, Cameroon
[5]Department of Civil Engineering and Architecture, National Advanced School of Engineering, University of Maroua, Maroua, Cameroon
Email: *zigla.abraham@enstp.cm

How to cite this paper: Zigla Atour, A., Taypondou, D.J., Todou Assaouka, H., Mabe Fogang, P., Zoua, V.P., Kouotou, P.M. and Yanné, E. (2026) Assessing the Suitability of Zimado Clay as a Precursor for Sustainable Lightweight Expanded Clay Aggregate (LECA) Production. *Journal of Materials Science and Chemical Engineering*, **14**, 30-57.
https://doi.org/10.4236/msce.2026.148003

Received: May 2, 2026
Accepted: August 8, 2026
Published: August 11, 2026

Copyright © 2026 by author(s) and Scientific Research Publishing Inc.
This work is licensed under the Creative Commons Attribution International License (CC BY 4.0).
http://creativecommons.org/licenses/by/4.0/
Open Access

Abstract

The supply of conventional aggregates represents a well-established major challenge in several landlocked localities of the Lake Chad Basin, particularly in the Zimado area, where such materials are typically sourced from quarries located at considerable distances. In response to this constraint, the present study aimed, for the first time, to carry out a comprehensive physical, chemical and mineralogical characterization of Zimado clay, with a view to assessing its thermal expansion potential for the production of lightweight aggregates via heat treatment. Three representative samples (ZC1, ZC2 and ZC3) were collected at a depth of 70 cm to ensure adequate spatial representativeness. These samples were subjected to particle size analysis (NF P 94-056/057), Atterberg limit determination (NF P 94-051) and absolute density measurement, alongside geochemical and mineralogical analyses including X-ray fluorescence (XRF), X-ray diffraction (XRD) and Fourier-transform infrared (FTIR) spectroscopy. The results reveal that Zimado clay exhibits a silty-clayey texture, with silt and clay fractions accounting for 41.41% and 24.84%, respectively, a moderate plasticity index ranging from 15.68% to 23.12%, and a mean absolute density of 2.409 g/cm^3. The chemical composition is predominantly aluminosilicate in nature, with SiO_2 contents ranging from 63.06 to 65.90 wt% and Al_2O_3 from 14.94 to 15.60 wt%. The mineralogical assemblage is dominated by quartz, kaolinite, illite, feldspars and ferruginous phases. Assessment

against Riley's (1951) expansion screening criteria indicates that two of the three compositional thresholds are met by the measured composition; only the total flux oxide content (~10.55 - 11.78 wt%) falls marginally below the recommended minimum of 13 wt%. Collectively, these results provide a first baseline characterization of Zimado clay and support its preliminary identification as a physicochemical promising precursor for lightweight expanded clay aggregate production; empirical validation through firing trials remains necessary before production suitability can be confirmed.

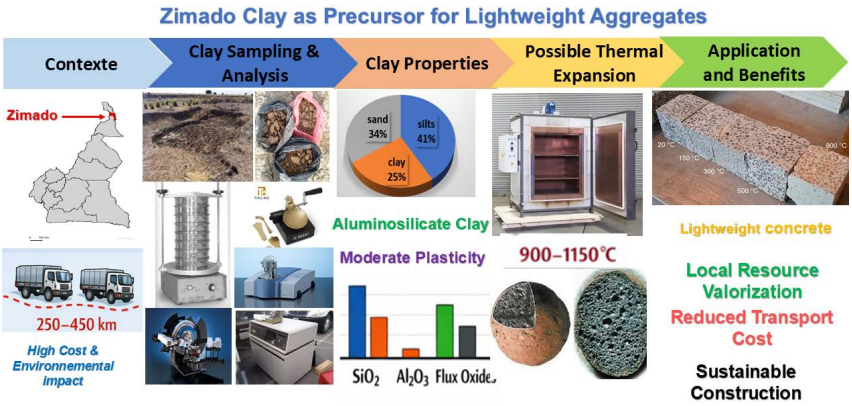

Keywords

Conventional Aggregates, Zimado Clay, Lightweight Aggregates, Characterization, Thermal Treatment, Bloating Criteria

1. Introduction

In the Far North Region of Cameroon, access to conventional construction aggregates is persistent constrain. In Zimado, a locality within the Logone-Birni subdivision, no hard rock deposit is available locally. Gravel must be transported from Mora or Waza approximately 250 km away, or form Moundou in Chad at 450 k, generating transportation costs that represent a substantial share of total project expenditure [1] [2]. Since aggregates account for 60% to 80% of concrete volume and directly govern its compressive strength, workability and durability [3], these logistics are not a secondary concern: they explain why school infrastructure and housing projects in the area frequently fail to reach completion [4]. The extraction of alluvial aggregates from local seasonal watercourses (mayos) has been explored as an alternative, but raises serious environmental concerns, accelerated bank erosion, destabilization of riparian zones, and increased flood risk that limit its viability [5] [6]. Zimado does, however, possess abundant clay-rich soils, currently exploited through artisanal techniques for fired bricks and ceramics. The plasticity of these clays, governed by their mineralogical composition and water content [7], makes them candidates for thermal expansion. Expanded clay produced by rapid firing at 900˚C - 1300˚C [8] is a lightweight porous aggregate whose density re-

duction dans controlled porosity confer thermal and acoustic insulation properties [9] [10] while retaining mechanical performance compatible with structural applications [11]. The expansion mechanism relies on the release of internal gases during vitrification, as described by Riley (1951) [12], and is governed by the mineralogical and chemical composition of the raw material: the presence of clay minerals (kaolinite, illite), quartz and fluxing oxides (Fe_2O_3, K_2O, CaO, MgO) influences the viscosity of the glassy phase and the condition under which gases are generated and trapped [13]-[18]. Producing expanded clay locally would reduce dependence on imported aggregates, lower transportation-related CO_2 emissions [19], and create a pathway for the circular valorization of a readily available geo-resource [20] [21]. However, none of this is achievable without a rigorous characterization of the raw material.

No prior published characterization of Zimado clays has been identified in the literature. This study provides the first reported physicochemical and mineralogical analysis of this material, combining particle size analysis, Atterberg limits, absolute density, XRF, XRD and FTIR, with the objective of assessing its suitability as a precursor for lightweight expanded clay aggregate production.

2. Methodology

2.1. Study Area

2.1.1. Localization, Climate

The study area is located in Zimado, a locality within the Logone-Birni subdivision in the Far North Region of Cameroon, situated at coordinates 11˚40'06" North and 15˚04'27" East. Figure 1 situated the site within this administrative

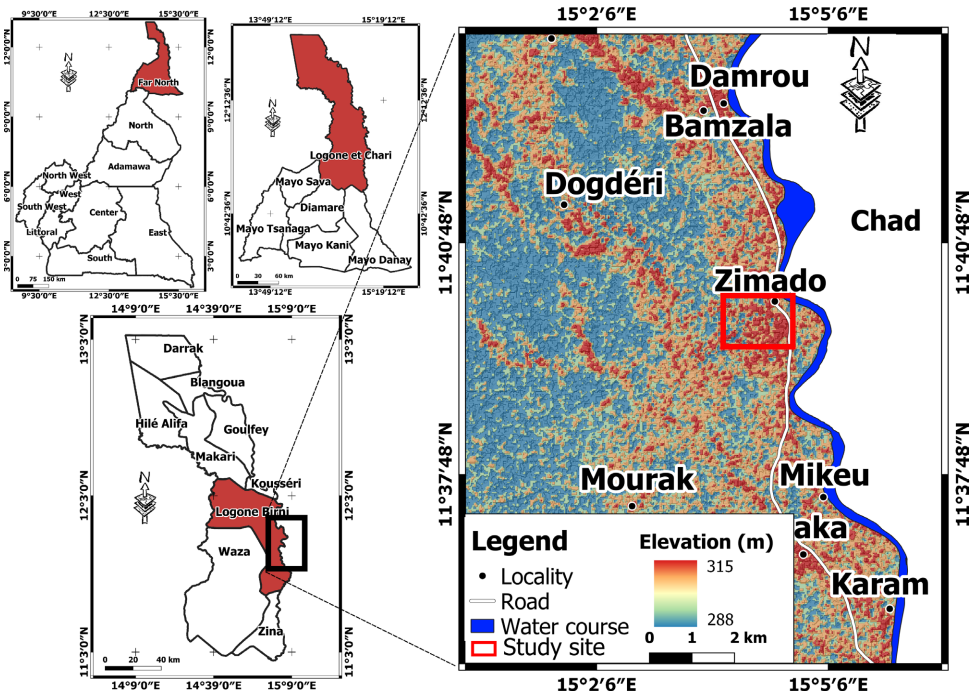

Figure 1. Location of the studied area in Cameroon.

hierarchy and shows its position relative to the local topography and hydrographic network, confirming its location immediately adjacent to the Logone River. The locality experiences a Sudano-Sahelian climate, characterized by the alternation of two seasons, a long dry season (October-June) and a short rainy season (July-September) [22]. The average recorded temperature is 29˚C, with April being the hottest month, reaching up to ~40.7˚C, and December the coldest, dropping to ~18.8˚C, with an average annual precipitation of 700 mm. The topography around Zimado and Logone-Birni is that of a flat floodplain (288 - 315 m altitude), forming part of the Chad Basin, dominated by the Logone River and its marshlands [23].

2.1.2. Geological Setting

Zimado lies within the Logone Birni Basin, an intracratonic basin of the West and Central African rift system covering approximately 27000 km^2 in northern Cameroon, formed by Mesozoic rifting and infilled by sediment ranging from the Neocomian to Quaternary [24]. At the surface, the basin is blanketed by Quaternary detrital sediments typical of the Chad Basin floodplain derived from the erosion of the Precambrian crystalline basement to the south and reworked by the Logone river and its seasonal tributaries (mayos) [25]. Comparable clay deposits in the region have been described as polygenic, combining a detrital quartz-feldspathic fraction with clay minerals formed during transport and post-depositional weathering [26]. The clay-rich horizons around Zimado have long been exploited artisanally [27].

2.2. Field Investigation and Sampling

The valorization of Zimado clay as a lightweight aggregate requires meticulous, multi-scale characterisation based on internationally recognized analytical techniques. The objective is to verify whether these raw materials exhibit the physical, mineralogical, and chemical properties compatible with the production of lightweight expanded clay aggregates (LECA) compliant with established technical standards [28].

The field investigation began with a phase of prospection and reconnaissance of areas known for artisanal exploitation of clay materials intended for the manufacture of fired bricks and ceramic products. As shown in **Figure 2**, the sampling pit was excavated within such an active artisanal extraction site, confirming the empirical suitability of the material for firing and ceramic production. The exposed profile shows a homogeneous, stone free clay horizon supporting the choice of a 70 cm sampling depth below the sandy topsoil in the Zimado II neighborhood, intended to avoid superficial disturbances and to obtain a more homogeneous material. The observed grey tint suggests either a mineral composition with low iron oxide content or the presence of organic matter, a characteristic frequently mentioned in recent studies on Sahelian clays [29].

The collected material (**Figure 2**, right) forms cohesive clumps rather than friable or sandy aggregates, a field level indication of the workability subsequently

Figure 2. Artisanal clay extraction site in Zimado II: open excavation pit with visible clay-rich horizon and raw brick units in the background.

quantified through the Atterberg limit tests. Three samples ZC1, ZC2 and ZC3 were collected from the same horizon at approximately 30 - 50 m spacing within the Zimado II neighborhood, centred on the respective site coordinates (11˚39'33.98"N, 15˚04'40.19"E; 11˚39'34.70"N, 15˚04'38.60"N; 11˚39'35.64"E, 15˚04'40.08"N). This sampling strategy was designed to capture the compositional variability of the accessible horizon while remaining within the boundaries of the active extraction zone, it does not constitute a systematic spatial survey of the full deposit extend, and the results should therefore be interpreted as representative of this specific profile rather than of the lateral and vertical variability of the Zimado clay deposit. Field reconnaissance allowed a preliminary appraisal of the spatial extent of the deposit. The clay bearing horizon currently exploited in the Zimado II neighborhood extends over an estimated area exceeding 50,000 m^2, as delineated by the boundaries of ongoing and historical artisanal extraction pits. Within the open excavation faces (**Figure 2**), the clay unit is exposed to a minimum thickness of 80 cm, without its base having been reached, since the pits are dug only to the depth required for artisanal brick production. On this basis, a conservative, order of magnitude volume of approximately 40,000 m^3 can be inferred for the currently identified extent of the deposit. This figure should be regarded as a lower bound, field-based estimate rather than a quantified reserve assessment: it does not account for any additional thickness below the exposed pit floor, nor for clay bearing horizons that may extend beyond the area currently under artisan exploitation. These preliminary finding suggest a deposit of sufficient extent to warrant further investigation for potential semi-industrial or industrial-scale exploitation.

The samples collected from the site were subjected to physical testing (particle size analysis, Atterberg limits and absolute density), physicochemical and mineralogical analysis.

2.3. Analytical and Experimental Methods

Analyses including physical analysis, X-Ray diffraction (XRD), Fourier transform

infrared spectroscopy (FTIR) and X-ray fluorescence spectroscopy (XRF) were carried out on the selected Zimado clay samples.

2.3.1. Physical Analyses

Physical analyses were performed on the samples in the Laboratory of Structure, Mechanics and Materials of the National Advanced School of Public Works in Yaoundé, Cameroon.

Particle size distribution was studied using a combined method involving sedimentation according to Stokes' law for the fine fraction (<80 μm) and dry sieving after washing for the coarse fraction (≥80 μm), in accordance with the respective standards NF P 94-057 and NF P 94-056. These analyses provide comprehensive particle size data that are essential for soil classification and for understanding the thermal behavior of clay.

The NF P 94-051 standard describes the methods for determining the Atterberg limits, such as the liquid limit (LL), the plastic limit (PL) and the plasticity index (PI). This analysis was carried out on the fine fraction (<400 μm) of the three samples in order to assess the consistency and plasticity, which enable evaluation of workability of clay materials in the presence of water to evaluate workability and anticipate volumetric behavior (shrinkage or swelling phenomena), in order to predict the dimensional stability of clays subjected to heat treatment. The NF P 94-054 standard method was used to determine the absolute density of the Zimado clays. This method involves measuring the particles volume, thereby eliminating the effects of voids and intergranular air.

2.3.2. Geochemistry Study by X-Ray Fluorescence Spectroscopy (XRF)

The chemical composition of Zimado clay was analyzed using X-ray fluorescence (XRF) spectroscopy. The experiment was carried out using a Philips PW 1404 dispersion spectrometer, located in the cement company laboratory (CIMENCAM, Figuil, Cameroon), which is affiliated with the Lafarge Group. This spectrometer enables the precise detection and quantification of oxides of the major elements in the clay when it is irradiated by an X-ray beam. The major oxides thus observed are expressed as a percentage by mass. The analytical results obtained are used to assess the clay's thermal expansion properties using the ternary classification diagram proposed by Riley.

2.3.3. Mineralogical Structure by X-Ray Diffraction (XRD) Analysis

Mineralogical characterization was performed using X-ray diffraction (XRD). Measurements were carried out on finely ground sample powders using a Bruker diffractometer (D8 Focus at 40 kV and 150 mA), generating Cu Kα radiation with characteristic wavelengths of λ_1 = 1.5406 Å and λ_2 = 1.5418 Å. The samples were analyzed in the 2θ angular range between 2˚ and 50˚, with a step size of 0.02˚ and a counting time of two seconds per step. The resulting diffractograms were used to identify the crystalline phases by comparison with reference patterns from the International Centre for Diffraction Data (ICDD). The identified mineral phases were then correlated with the chemical composition to provide a comprehensive

picture of the physicochemical nature of the clay.

2.3.4. Fourier Transform Infrared (FT-IR) Spectroscopy

The chemical bonds and surface functional groups present in Zimado clay were identified using Fourier-transform infrared spectroscopy (FTIR). The instrument used was a Bruker ALPHA spectrometer. The infrared spectra were recorded in the spectral range from 250 to 4000 cm^{-1} with a spectral resolution of 4 cm^{-1}. The absorption bands thus obtained were systematically attributed to specific vibrational modes and interpreted in relation to the mineralogical phases previously identified by XRD analysis, thereby providing additional information on the molecular-scale structure of the clay.

2.3.5. Integrated Characterization Approach

All these analyses aim to verify the potential compliance of the material with the normative requirements applicable to structural lightweight aggregates, particularly concerning mechanical strength, density, and durability. This integrated approach, combining physical, mineralogical, and geochemical analyses, aligns with current recommendations for the sustainable valorization of local resources in construction materials. Thus, the adopted methodology does not merely constitute a preliminary technical step; it represents the essential scientific foundation for considering the transformation of Zimado clay into a high-performance lightweight aggregate, adapted to contemporary structural and environmental constraints.

3. Results

3.1. Geotechnical Results

The results of the Atterberg limit test are presented in **Table 1**. The liquid limit (LL) ranged from 42.09% to 50.96% while the plastic limit (PL) ranged from 26.41% to 29.03%. The plasticity index (PI) values were 17.75%, 15.68% and 23.12% for samples ZC1, ZC2 and ZC3 respectively. These liquid limit values indicate that these clays required a moderate water content to transition from a plastic to liquid state [30]. According to the diagram of Holtz and Kovacs (1981) [31] presented in **Figure 3**, all three samples classify as medium-plastic clay. ZC1 and ZC2 plot well within this range, whereas ZC3, owing to its higher plasticity index (23.12%), lies close to the boundary with the highly plastic domain. More notably, the three samples plot within the transition zone between the kaolinite and illite bands, providing an independent, plasticity-based confirmation of the kaolinite and illite mineral assemblage identified par XRD and FTIR. None of the samples approach the montmorillonite domain, consistent with the absence of any swelling clay phase in the XRD pattern. This medium-plasticity, kaolinite-illite dominated behavior supports adequate workability for granule forming while limiting the risk of excessive shrinkage during drying and firing.

The absolute particle density of the raw Zimado clays, measured by the pycnometer method ranges from 2.400 g/cm^3 to 2.421 g/cm^3, with an average value

Table 1. Physical properties of studied clays samples from Zimado.

	Studied clay samples				
	ZC 1	ZC2	ZC3	average	Std. Dev
	Atterberg limit and water content (%)				
Liquid limit (LL)	46.78	42.09	50.98	46.61	4.45
Plastic limit (PL)	29.03	26.41	27.86	27.77	1.31
Plastic Index (IP)	17.75	15.68	23.12	18.85	3.84
Water content	9.85	6.45	9.50	8.6	1.87
Absolute density (g/cm^3)	2.421	2.400	2.406	2.409	0.011
	Particle size distribution (%)				
Clay: (<0.002 mm)	25.42	24.57	24.53	24.84	0.50
Silt: (0.002 - 0.02 mm)	40.60	41.86	41.78	41.41	0.71
Sand (0.02 - 2 mm)	33.92	33.45	33.56	33.64	0.25
Gravel (>2 mm)	0.06	0.12	0.13	0.10	0.04

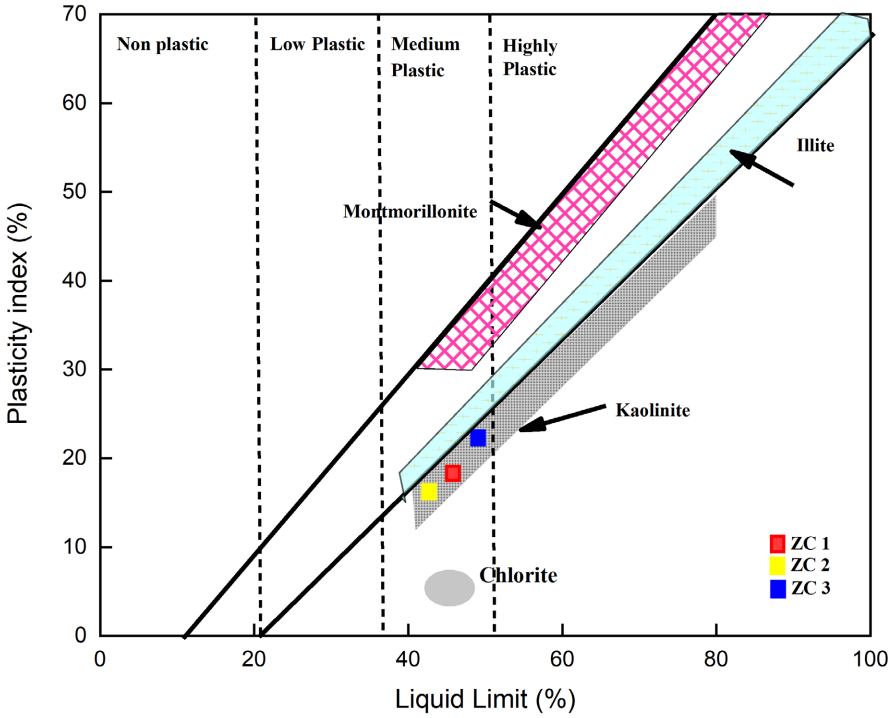

Figure 3. Position of Zimado clay samples (ZC1, ZC2 and ZC3) in the Diagram of Holtz and Kovacs.

of 2.409 g/cm^3. This average value is consistent with the absolute densities reported for clays dominated by kaolinite and/or illite, which typically vary between 2.4 and 2.7 g/cm^3 [32] [33].

The Zimado clay samples were subjected to comprehensive particle size analysis to characterise the distribution of textural fractions, in accordance with estab-

lished protocols for the granulometric characterisation of fine-grained soils [34]. Full results for the three samples, together with mean values and standard deviations for each fraction, are reported in **Table 1**, following the presentation format conventionally adopted in fine particle size studies [35].

As shown in **Figure 4**, all three samples exhibited a cumulative passing fraction through the 80 µm sieve in excess of 95% (97.94% for ZC1, 95.35% for ZC2 and 95.05% for ZC3), reflecting a predominantly fine-grained composition consistent with clayey and silty-clayey materials documented in Central Africa and the Lake Chad Basin [36] [37]. This fine and relatively uniform grain size is favorable for expanded aggregate production, as it promotes homogenous heat transfer and uniform gas generation throughout the pellet during firing, limiting the risk of localized, premature gas escape.

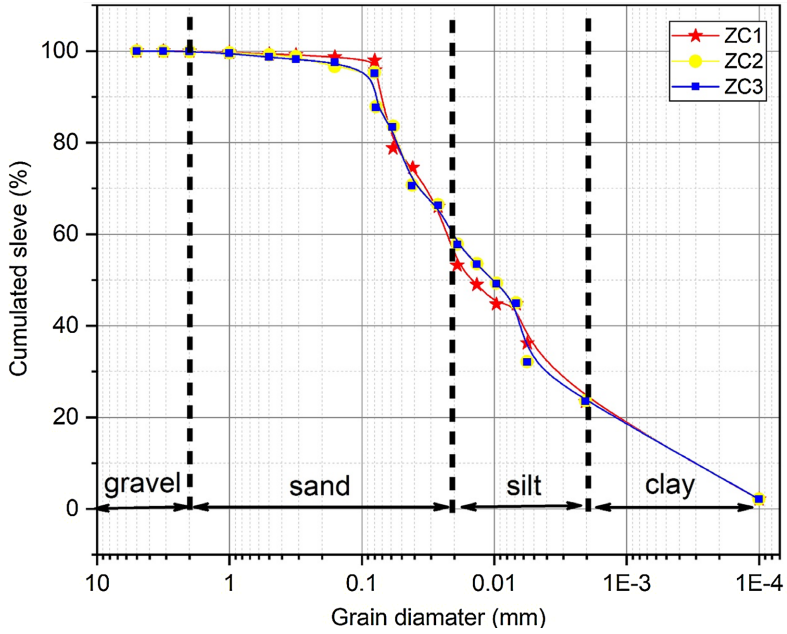

Figure 4. Particle size distribution curves of Zimado clay samples (ZC1, ZC2, ZC3).

Textural fraction analysis revealed a predominance of silt, accounting for a mean proportion of 41.41%, followed by sand (33.64%) and clay (24.84%). This distribution is characteristic of silty-clayey textures reported in several investigations of fine-grained soils from semi-arid and lacustrine environments [38] [39]. Notably, the silt-sized fraction largely composed of quartz and feldspar particles rather than clay mineral proper, as confirmed by XRD exceeds the clay fraction itself. This distinction does not detract from the material's expansion potential, quartz contributes to the structural rigidity of the pellet during firing, while feldspar acts as the principal fluxing agent promoting vitrification. The fine-grained fraction as whole therefore plays a functional role in the expansion process alongside the clay-mineral assemblage (kaolinite, illite) responsible for plasticity and internal gas generation.

The low standard deviations observed across the three samples for each textural

fraction confirm the relative compositional homogeneity of the Zimado clay deposit, a feature analogous to the textural uniformity described in fine-grained lacustrine and alluvial sedimentary systems [40] [41]. This homogeneity supports a consistent behavior during forming and firing, though it contrasts with the greater variability observed in plasticity index.

3.2. Chemical Composition of the Sample by XRF

The chemical composition of the Zimado clay was determined by X-ray fluorescence (XRF) spectrometry. The elemental analysis results, illustrated in **Table 2**, reveal a material predominantly composed of silica (SiO_2 ranging from 63.058 to 65.896 wt%) and alumina (Al_2O_3 ranging from 14.935 to 15.598 wt%), accompanied by moderate proportions of iron oxide (Fe_2O_3 ranging from 2.699 to 2.863 wt%), magnesium oxide (MgO ranging from 2.056 to 2.063 wt%), sodium oxide (Na_2O ranging 2.220 to 2.478 wt%), potassium oxide (K_2O ranging from 1.067 to 2.081 wt%), calcium oxide (CaO ranging from 2.343 to 2.506 wt%), and titanium dioxide (TiO_2 ranging from 1.080 to 1.089 wt%). Minor constituents including P_2O_5, SO_3, and Mn_2O_3 were observed. Zimado's high SiO_2 and notable Al_2O_3, together with moderate Fe_2O_3 and flux oxides and minor P_2O_5, SO_3, Mn_2O_3, closely mirror compositions reported for clay formations from Gaschiga [42], Sekandé [42], Boulgou [43], South Mindif [44], Makabaye [45] and Yagoua [45] [46], all

Table 2. Chemical composition of studied clay samples from Zimado.

	Studied clay samples		
	ZC1	ZC2	ZC3
SiO_2	63.058	65.896	63.225
CaO	2.343	2.506	2.435
Fe_2O_3	2.863	2.699	2.746
Al_2O_3	15.386	15.598	14.935
MgO	2.065	2.063	2.056
K_2O	2.081	1.067	2.033
Na_2O	2.435	2.22	2.478
SO_3	0.125	0.118	0.185
Mn_2O_3	0.078	0.098	0.068
ZnO	0.703	0.718	0.795
P_2O_5	0.755	0.768	0.738
TiO_2	1.080	1.089	1.095
LOI	7.027	5.159	7.210
Total	99.999	99.999	99.999
SiO_2/Al_2O_3	4.098	4.225	4.233
Flux (Fe_2O_3+ CaO+ MgO+ K_2O+ Na_2O)	11.787	10.555	11.748

characterized as aluminosilicate clays [44] [47].

3.3. Fourier-Transform Infrared (FTIR) Spectroscopy Analysis

Fourier transform infrared spectroscopy (FTIR) analysis of the Zimado clay samples, recorded in the 4000 - 400 cm^{-1} range, reveals several characteristic absorption band typica of clay mineral like OH and Si – O/Al – O that confirm the predominantly aluminosilicate nature of the samples, in agreement with the oxide composition results obtained by X-ray fluorescence (XRF) [48] [49]. The corresponding spectra are presented in Figure 5.

- ***O-H Stretching Vibration Region*** **(3200 - 3600 cm^{-1})**

The broad band centered at ~3343 cm^{-1} corresponds to O-H stretching of structural hydroxyl groups (Si-OH, Al-OH) in kaolinite and adsorbed water [50] [51], consistent with the Al_2O_3 content and LOI determined by XRF. Both kaolinite and illite contribute to this band, although the shared nature of this spectral region does not allow their individual contribution to be resolved without deconvolution. Similar results have been reported for kaolinitic, and illitic clays from the Lake Chad Basin [37] [52] [53].

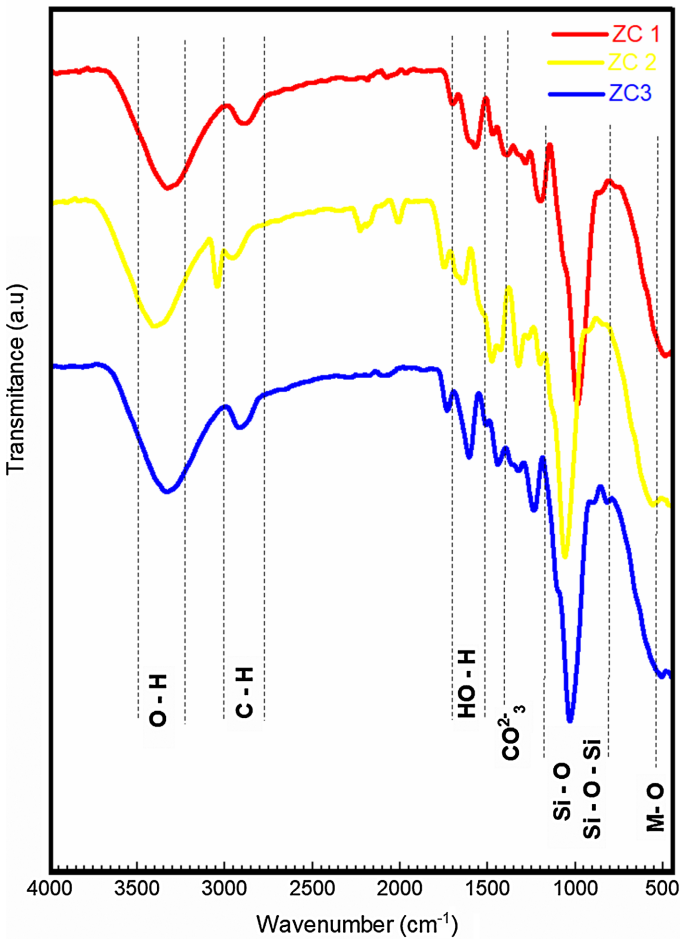

Figure 5. Diffuse reflectance infrared Fourier transform spectroscopy patterns of Zimado Clay.

- ***C-H Band*: *Organic Matter* (~3000 - 2850 cm^{-1})**

The bands in the 3000 - 2850 cm^{-1} range (-CH_3/-CH_2-) confirm the presence of organic matter in the Zimado clay [54], consistent with part of the measured LOI. Its decomposition between 300˚C and 550˚C releases CO_2/CO, contributing to the gas supply require for bloating [55] [56].

- ***Adsorbed water signature* (~1630 cm^{-1})**

The band at ~1630 cm^{-1} reflects H-O-H deformation of water adsorbed on the silica-alumina surface [57] [58], consistent with the high SiO_2 contents measured by XRF [59] [60].

- ***Carbonate region* (~1450 cm^{-1})**

The moderate intensity bands near 1450 cm^{-1} indicates trace carbonates (CO_3^{2-}) [61], consistent with the low CaO content from XRF and the absence of a strong calcite band near 875 cm^{-1} [62].

- ***Dominant Silicate Network Band* (~1035 cm^{-1} and 890 cm^{-1})**

The intense band at ~1035 cm^{-1} (Si-O asymmetric stretching) [63], and the weaker band at 890 cm^{-1} (Si-O-Si symmetric stretching) [64], form the dominant silicate signature, in line with the high SiO_2 content from XFR.

- ***Low-Frequency Region* (~426 cm^{-1})**

The band near ~ 426 cm^{-1} fall in a region associated with metal-oxygen and Si-O/Al-O deformation modes [65].

3.4. Mineralogical Composition by X-Ray Diffraction Analysis

X-ray diffraction (XRD) analysis of the Zimado clay samples, recorded between 5˚ to 50˚ (2θ), is illustrated in **Figure 6**. A semi-quantitative ordering of mineral phase abundance, based on relative peak heigh across the three diffractograms, is provided directly in **Figure 6**. Quartz is identified as the clearly dominant phase,

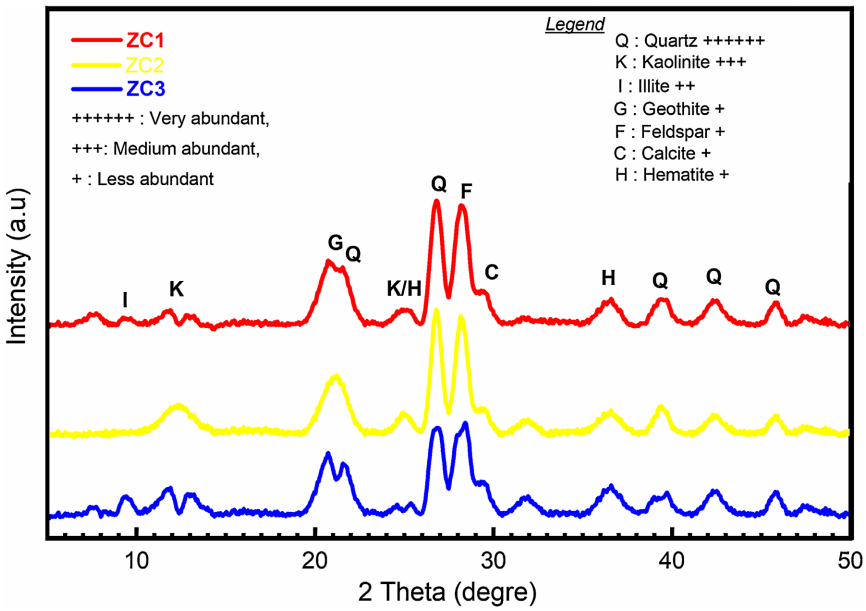

Figure 6. XRD spectrum of Zimado clay.

followed by kaolinite as the main clay mineral constituent. Illite is present as a minor to intermediate accessory phase, while goethite, feldspar, calcite and hematite all occur in subordinate proportions. This ordering is based on visual peak height comparison rather than Rietveld refinement analysis, this assemblage is characteristic of sedimentary clays from the Lake Chad Basin [53] [66].

- ***Quartz***

Quartz constitutes the dominant mineral phase of the Zimado clay samples, attested by the most intense diffraction peak in the diffractogram, located at $2\theta \approx 26.6^\circ$, corresponding to the characteristic (101) reflection of this phase (JCPDS file No. 46-1045) [67]. Several secondary peaks of lesser intensity are observed for all the samples, unambiguously confirming the identification of quartz as the majority phase. This predominance is fully consistent with the high SiO_2 determined by XRF and with the intense Si-O (~1035 cm^{-1}) and Si-O-Si (~890 cm^{-1}) absorption bands identified by FTIR. Similar results have been reported for sedimentary clays from the Lake Chad region [68].

- ***Kaolinite***

The basal peaks of the samples observed at $2\theta \approx 12.3^\circ$ correspond to the (001) reflection characteristic of kaolinite, confirming the presence of this clay mineral as a major phase. The secondary reflection at 24.89° (002) reinforces this attribution, although it partially overlaps with a hematite reflection in the same angular range, as indicated **Figure 6** [69] [70]. The moderate intensity of the basal peak indicates kaolinite of medium crystallinity, consistent with a detrital origin and post-depositional alteration during fluvial transport describe in Section 2.1.3, rather than a hydrothermal mode of formation. The significant presence of kaolinite is consistent with the Al_2O_3 content determined by XRF as well as with the O-H band observed in FTIR (~3400 cm^{-1}), attributed to structural hydroxyl groups. The presence of kaolinite is technologically significant because its dehydroxylation between 450 and 600˚C, leading to the formation of metakaolinite, generates structural water capable of contributing to internal gas pressure during firing, thus participating in the bloating mechanism [55].

- ***Illite***

A low intensity reflection at $2\theta \approx 9.1^\circ$ correspond to the (001) basal spacing illite, confirming its presence as a minor accessory phase alongside kaolinite [71]. A harmonic reflection near $2\theta \approx 17.7^\circ$ was not unambiguously resolved, likely due to the low illite content and overlap with other phases. The low intensity of this peak, relative to the kaolinite and quartz reflections, indicates that illite occurs in subordinate proportion within the clay mineral assemblage. This is consistent with O-H band observed in FTIR (~3343 cm^{-1}), to which both kaolinite and illite contribute.

- ***Feldspars***

The reflection at $2\theta \approx 28.3^\circ$ distinct from the dominant quartz peak at 26.6° by its lower intensity and slightly different d-spacing, is consistent with K-feldspar, specifically microcline [72]. However, the Na_2O content measured by XRF (2.22 -

2.48 wt%, comparable to K_2O in ZC1 and ZC3) raises the possibility of co-occurring plagioclase feldspar, whose diagnostic reflections overlap significantly with those of K-feldspar in this angular range and cannot be distinguished without single-crystal diffraction or electron microprobe analysis. The feldspar attribution is therefore retained as a mixed K-feldspar/plagioclase assignment. Both phases act as fluxing agents during firing, promoting the formation of a vitreous phase [73].

- ***ferruginous phases***

A reflection near 21.2˚ is tentatively attributed to the goethite according to the files (JCPDS: 00-003-0249) [74], although it partial overlaps with a secondary quartz reflection at ~20.8˚ and the relatively low Fe_2O_3 content (2.70 - 2.86 wt%) make unambiguous identification without peak profile fitting difficult. This attribution is supported by the presence of Fe_2O_3 in XRF, but should be regarded as possible rather than confirmed pending higher resolution XRD. Goethite is a common ferruginous phase in lateritic or slightly weathered clays. During heating, it transforms into hematite (Fe_2O_3), thereby contributing to the vitrification properties and the red coloration of the material. Hematite is not directly identified as a discrete phase at room temperature in the diffractograms; its presence is inferred from the K/H label assigned to the reflection near $2\theta \approx 24.89^\circ$, where it partially overlaps with the kaolinite (002) reflection, and from the Fe_2O_3 content measured by XRF. Its occurrence at room temperature is therefore considered tentative; it may represent a secondary oxidation product of goethite formed during sample drying and preparation. During thermal treatment, the goethite-to-hematite transformation (250˚C - 400˚C) is expected to produce the discrete hematite phase responsible for the characteristic red coloration of fired clay products.

- ***Possible Traces of Calcite***

A low-intensity reflection near $2\theta \approx 29.5^\circ$, consistent with the characteristic (104) reflection of calcite (JCPDS 05-0586), suggests the presence of trace carbonate. The low intensity of this peak and the low CaO content measured by XRF (2.34 - 2.51 wt%) confirm that calcite constitutes a minor secondary phase only. This attribution is further supported by the low-intensity CO_3^{2-} absorption band at ~1450 cm^{-1} in FTIR and is consistent with the moderate LOI, indicating a limited carbonate contribution to total mass loss.

4. Discussion

4.1. Physical Parameter

Producing expanded clay requires sufficient plasticity to form cohesive granule capable of retaining interstitial water, which generates the internal gases driving expansion during firing [75] [76]. The plasticity index measured for Zimado clay (15.68% - 23.12%, **Table 1**) falls withing the medium-plasticity range reported for clay successfully processed into LECA without additives [77], indicating adequate workability and granule cohesion for the forming stage while remaining moderate enough to limit shrinkage cracking during firing. As emphasized in recent reviews, the plasticity and density of the raw material ultimately condition the ex-

pansion, porosity and mechanical performance of the fired aggregate [78].

4.2. Physicochemical and Mineralogical Analysis

4.2.1. Assessment of Thermal Expansion Potential Based on Chemical Composition: Riley Criteria

The suitability of Zimado clay for the production of expanded lightweight aggregates was evaluated using two complementary approaches widely employed in the literature: the individual criteria proposed by Riley (1951) [12] and the synthetic Expansion Index R = SiO_2/Flux.

- **Riley's Individual Criteria (1951)**

The chemical composition of Zimado clay was assessed against Riley's (1951) criteria with results presented in **Table 3** and **Figure 7**. On the SiO_2-Al_2O_3 plane (**Figure 7**, left), all three samples plot well within the bloating zone, a robust result that holds across the deposit. On the SiO_2-Flux plane (**Figure 7**, right), however, all three samples fall below the lower boundary of the bloating zone, confirming a systematic deficit in fluxing oxides. The deficit is not uniform: ZC1 and ZC3 fall approximately 1.2 wt% below the 13% threshold, while ZC2 the most flux-deficient sample falls 2.4 wt% short.

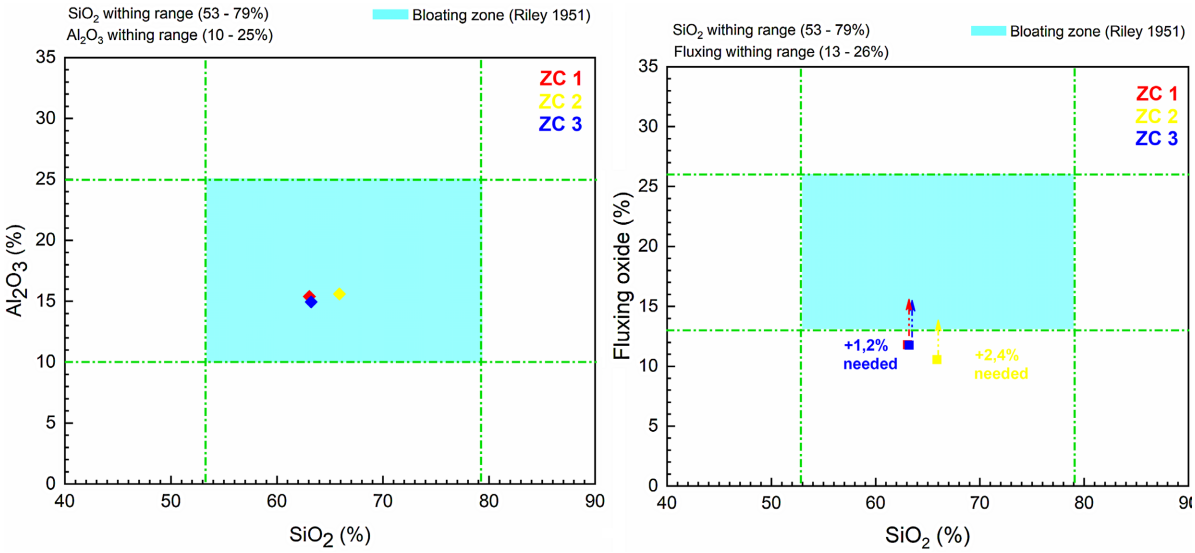

Figure 7. Zimado clay plotted on Riley's (1951) Bloating diagram.

This insufficiency in fluxing oxides suggests that, under standard firing conditions, the pyroplastic melt may exhibit excessively high viscosity, limiting the entrapment of gases generated by organic matter combustion and carbonates decarbonation a central mechanism in the bloating process described by some authors [55] [79]. It should be noted, however, that both deficits are narrow and concern a single parameter, the SiO_2-Al_2O_3 balance is already favorable, meaning flux correction would not require reformulating the bulk composition but only supplementing the existing assemblage. In practice, an addition somewhat above the calculated minimum in the order of 2 - 3 wt% would provide a reasonable safety

margin against compositional heterogeneity within the deposit, rather than positioning the corrected material exactly at the lower boundary of the bloating zone. The precise addition required for Zimado clay remains to be determined experimentally through firing trials.

- ***Expansion Index R = SiO_2/Flux***

The Riley's individual criteria can be complemented by a single expansion index *R*, defined as the ratio of silica to the sum of fluxing oxides (**Table 3**).

$$R = \frac{SiO_2}{Flux}$$

This index reflects the balance between the network-forming component (SiO_2, which governs melt viscosity) and the network-modifying components (fluxing oxides, which collectively control fluidity and structural stability at high temperatures) [21] [80]. For the Zimado clay samples R ranges from 5.35 to 6.24, well below the upper threshold of 9 reported as favorable for bloating [81]. This indicates that despite the marginal deficit in fluxing oxides in absolute terms (**Table 3**), the overall compositional balance between silica and network modifiers remains favorable for thermal expansion.

Taken together, the absolute Riley criteria indicate that the Zimado clay satisfies two of three compositional requirements, with a narrow, single parameter deficit in flux content, while the silica to flux ration remain within a range generally associated with favorable bloating behavior. On this basis, Zimado clay is classified as compositionally borderline-favorable for bloating, with the absolute flux deficit identified as the primary corrective target. This classification should be regarded as a working hypothesis requiring confirmation through experimental firing trials, insofar as Riley's criteria and the derived expansion index constitute preliminary screening tools that cannot substitute for direct empirical demonstration of bloating behavior.

Table 3. Assessment of the thermal expansion potential of Zimado clay according to the chemical criteria of Riley (1951).

Chemical composition	Studied clay samples				
	ZC1	ZC2	ZC3	Required criteria	status
SiO_2	63.058	65.896	63.225	53 - 79	satisfied
Al_2O_3	15.386	15.598	14.935	10 - 25	satisfied
Flux (Fe_2O_3 + CaO + MgO + K_2O + Na_2O)	11.787	10.555	11.748	13 - 26	Bellow lower limit
SiO_2/Al_2O_3	4.098	4.225	4.233		Aluminosilicate-dominated matrix
Expansion index $R = SiO_2$/Flux	5.350	6.243	5.382	<9	satisfied

4.2.2. XRD-XRF-FTIR Correlation

The both analytical techniques converge towards a coherent interpretation of the material's nature:

- *XRD-XRF Correlation*

The high SiO_2 content measured by XRF is confirmed by the dominant intensity

of the quartz peak in XRD. The presence of kaolinite is consistent with the significant Al_2O_3 content. The alkali oxides (Na_2O, K_2O) detected by XRF correspond to the presence of feldspars. The Fe_2O_3 content is compatible with the presence of goethite and hematite detected by XRD.

The overall chemical composition is consistent with the mineralogical analysis.

- *XRD-FTIR Correlation*

The hydroxyl groups observed in FTIR (~3400 cm^{-1}) confirm the presence of kaolinite identified by XRD. The intense Si-O-Si band (~1035 cm^{-1}) corresponds to the silicate network of quartz and silicates. The weak carbonate band (~1450 cm^{-1}) is consistent with the possible traces of calcite detected by XRD.

FTIR therefore provides functional and structural confirmation of the crystalline phases identified by XRD.

4.3. Prediction of Zimado Clay's Expansion Properties

The complete dataset obtained from the physicochemical, physical and mineralogical characterization enables the evaluation of the Zimado clay with respect to its suitability for the production of expanded lightweight aggregates. This suitability is assessed using a multi-criteria approach, and the results are presented in **Table 4** [82]. The analyses of physicochemical composition, mineralogy and physical properties systematically complement one another, demonstrating a high level of internal consistency that strengthens the overall dataset.

A fine granulometry (a dominant fraction below 80 μm exceeding 95%) and uniform particle size distribution promote initial compactness and homogeneity during shaping [83] [84], which is a prerequisite for uniform expansion. A moderate plasticity index (Ip between 15% and 23%) reflects an optimal balance between cohesion and workability [84] [85], ensuring efficient forming without excessive cracking.

Silica in the Zimado clay occurs in two forms: predominantly as crystalline quartz and as structurally bound silica within phyllosilicates such as kaolinite and illite [86] [87]. This dual occurrence is favourable for expansion, as quartz contributes to the rigidity and stabilization of the skeletal structure of the clay pellets by remaining refractory at relatively low temperatures [88] [89], whereas phyllosilicates participate in the formation of a vitreous phase from approximately 950˚C [89]. Alumina associated with phyllosilicates ensures partial refractoriness and prevents structural collapse of the pellets during expansion.

Loss on ignition (LOI) is a key parameter in the production of expanded aggregates. Based on the obtained data, it can be decomposed into three contributions: 1) dehydroxylation of kaolinite as the primary contribution [90], 2) combustion of organic matter as the secondary contribution (confirmed by C-H bands) [91], and 3) minor decarbonation of carbonates (confirmed by the presence of CaO and CO_3^{2-} absorption bands) [92]. These three sources of gas release, typically occurring over successive and complementary temperature ranges, generate progressive internal pressure, which is an ideal condition for homogeneous expansion without

rupture of the vitreous shell [93] [94].

Feldspars act as the principal fluxing agents, lowering the onset temperature of vitrification (850˚C - 900˚C) [95]. In the absence of fluxes, a vitreous phase would not form, allowing gases to escape freely. The goethite present transforms into hematite between approximately 250˚C and 400˚C, releasing structural water [96]. During the vitrification stage, Fe^{3+} may be reduced to Fe^{2+}, generating additional oxygen. The presence of Fe_2O_3 is therefore favourable for expansion, as it plays a dual role as both a secondary flux and a gas-generating agent [97].

Proposed thermal transformation model

Based on XRD, FTIR and XRF data, the following sequence represents a predicted firing behavior inferred from room-temperature analytical data. Each step requires validation through TGA/DTA/DSC and firing trials before it can be treated as an established result.

Step 1 (ambient to 300˚C): Removal of adsorbed water (FTIR band at ~1630 cm^{-1}) and interlayer water from possible illitic phases. The clay pellets are predicted to undergo initial shrinkage and consolidation, with no expansion is expected at this stage.

Step 2 (300˚C - 550˚C): Combustion of organic matter (C-H bands at 2850 - 3000 cm^{-1}) is expected to release of CO_2 and CO. Within the same temperature range, the tentatively identified goethite is predicted to transforms into haematite with the release of structural water. As this stage, gases are not expected to be trapped, as no vitreous phase is predicted to have formed yet.

Step 3 (450˚C - 650˚C): Dehydroxylation of kaolinite, consistent with XRD and FTIR data, is expected to lead to the formation of metakaolinite. This transition is predicted to be critical, as metakaolinite is generally the most reactive intermediate phase and is expected to serve as a precursor for vitreous phase formation at higher temperatures.

Step 4 (850˚C - 1000˚C): Onset of vitrification through melting of alkaline fluxes (feldspars) is predicted to begin in this range. The emerging vitreous phase is expected to progressively seal the surface of the clay pellets, trapping residual gases. This step is predicted to mark the beginning of measurable expansion, though the precise onset temperature for Zimado clay remains to be determined experimentally.

Step 5 (1000˚C - 1150˚C): Maximum expansion is predicted to occur in this range, corresponding to near-optimal melt viscosity. Residual and dissolved gases (CO_2 from decarbonation and O_2 from $Fe^{3+} \rightarrow Fe^{2+}$ reduction) are expected to inflate the internal structure. The SiO_2/Al_2O_3 ratio (4.10 - 4.23) suggest a melt viscosity that may be sufficiently fluid to deform while remaining viscous enough to prevent structural collapse.

Step 6 (>1150˚C): Formation of mullite, which would contribute to the final mechanical strength of the aggregate, is expected at this stage.

This proposed model provides a testable framework for future experimental work. Firing trials across the 900˚C - 1150˚C range, combined with TGA/DTA

and post-firing XRD, are required to confirm, refine, or revise each predicted step for this specific clay. Table 4 summarises the multi-criteria suitability assessment across the four parameter categories examined in this study. Of the twelve parameters assessed, eleven return a favorable or very favorable rating. Taken together, the physicochemical and mineralogical data support a preliminary classification of Zimado clay as compositionally favorable for lightweight aggregate production on most assessed parameters, with a marginal flux deficit.

Table 4. Summary of correlations for the expansion term.

Category	Parameter	Observed value	Role in expansion	assessment
Chemical composition	SiO_2/Al_2O_3 ratio	4.098 - 4233	Controls glass transition viscosity during firing	Favorable
	Alkaline flux (K_2O + Na_2O)	3.287 - 4.511	Reduces vitrification temperature	Favorable
	Fe_2O_3	2.699 - 2.863	Secondary flux; releases O_2 during firing	Favorable
	CaO	2.343 - 2.506	Minor CO_2 source via calcite decomposition	Favorable
	MgO	~2.06	Minor flux;	Favorable
	Total flux	10.555 - 11.787	Below Riley's 13% threshold	Borderline. Correction addition required
Mineralogy	Kaolinite	Detected by XRD/FTIR	Dehydroxylation (450˚C - 600˚C) generates structural water and internal gas	Very favorable
	Calcites traces	Detected by XRD/FTIR	CO_2 release during firing	Favorable
	Organic matter	Detected by FTIR	CO_2/CO release early-stage expansion	Favorable
Physical properties	Plasticity index (Ip)	15.68% - 23.12%	Medium plasticity ensures uniform granule forming	Favorable
Compositional screening	Riley's diagram position	2/3 criteria satisfied	Overall compositional proximity to bloating zone	Borderline – favorable
	Expansion index R	5.350 - 6.243	Well below upper threshold	Favorable

4.4. Limitations of the Study

This work is subject to a certain limitation and we took into consideration when interpreting the results. First, the characterization is based on three samples collected from a single site and taken at approximately the same depth (70 cm); it therefore reflects the properties of this specific profile rather than the full lateral and vertical variability of the Zimado clay deposit, and any inference regarding the extend of exploitable reserves should be treated as preliminary pending a broader sampling campaign. Second, the assessment of bloating potential relies entirely on indirect chemical and mineralogical screening criteria, Riley's bloating diagram and the SiO_2/flux expansion index. No firing trial was performed in this study; consequently, the six-stage thermal transformation sequence proposed in

section 4.3 constitutes a model inferred from analytical data rather than an experimentally verified results, and the actual swelling behavior of Zimado clay remains to be confirmed by laboratory firing tests. Third, mineral phase identification by XRD was qualitative, without Rietveld refinement, the relative dominance of phases reported here therefore reflects peak intensity rather than quantified mass fraction, and the attribution of certain minor spectral features (notably the ZnO related FTIR band) should be regarded as tentative given their low concentration and overlap with major aluminosilicate band. Finally, loss on ignition was derived as a single bulk value from XRF rather than form a continuous thermogram, and no certified reference material was reported for XRF calibration. These limitations do not affect the validity of the characterization data presented, but the define the scope within which the conclusions on thermal expansion suitability should be read, and the delineate the experimental work, such as firing tests, TGA/DTA/DSC, and XRD quantified by the Rietveld method.

5. Conclusions

Zimado clay is here subjected, for the first time, to a comprehensive physicochemical and mineralogical characterization using particle size analysis, Atterberg limits XRF, XRD and FTIR, the full dataset presents a coherent: a silt-clay aluminosilicate of intermediate plasticity, whit mineralogical assemblage dominated by kaolinite, quartz, feldspars, and ferruginous phases.

Examination against Riley's criteria reveals a key weakness: the flux oxide content (10.56 - 11.79 wt%), fall below the recommended minimum of 13 wt%, which may limit the fluidity of the glassy phase under standard firing conditions. Two of three original Riley criteria are satisfied, and the expansion index R (5.35 - 6.24) remains within the favorable range, placing Zimado clay in a compositionally borderline-favorable position with a narrow, single-parameter deficit as the sole corrective target.

In terms of scientific contribution, this research expands the available database on sedimentary clays from the Lake Chad Basin and provides a first quantitative assessment of Zimado clay's expansion potential. Three research direction warrant priority investigation. The first is experimental: firing tests should be carried out at temperatures ranging from 900˚C to 1150˚C in order to empirically verify bloating behavior. The second, a targeted flux correction strategy: while the Zimado clay satisfies two of Riley's three criteria original compositional and presents a favorable silica-to flux ratio (R = 5.35 - 6.24), the marginal flux oxide deficit suggest a compensatory strategy, including flux addition (e.g., 1.2 - 2.4 wt% of Fe_2O_3 or feldspar). The third is analytical: a coupled DTA-TGA analysis to map the thermal transformation sequences and refine the firing parameters with a view to semi-industrial application.

Acknowledgements

The authors gratefully acknowledge research support by individual and we would

like to thank the Laboratory of Mechanics, Materials, Geotechnics, and Structures of the National Advanced school of Public Works, Yaoundé for the Physical Analysis.

Data Availability Statement

All data generated or analyzed during this study are included in this published article.

Author Contributions

Abraham Zigla Atour: Conceptualization, Methodology, Formal analysis, Investigation, Writing—original draft, Writing—review & editing, Visualization.

Darman Japhet Taypondou: Investigation, Writing—review & editing.

Hippolyte Todou Assaouka: Writing—review & editing.

Pieride Mabe Fogang: Writing—review & editing.

Vincent de Paul Zoua: Writing—review & editing.

Patrick Mountapmbeme Kouotou: Writing—review & editing, Project administration.

Etienne Yanné: Writing—review & editing.

Conflicts of Interest

The authors declare that they have no conflict of interest.

References

[1] Dominguez, C. and Foster, V. (2011) Cameroon's Infrastructure: A Continental Perspective. https://doi.org/10.1596/1813-9450-5822

[2] Tažiková, A. and Struková, Z. (2021) The Impact of Logistics on the Cost of Prefabricated Construction. *Acta Logistica*, **8**, 65-71. https://doi.org/10.22306/al.v8i1.204

[3] Berredjem, L., Arabi, N. and Molez, L. (2020) Mechanical and Durability Properties of Concrete Based on Recycled Coarse and Fine Aggregates Produced from Demolished Concrete. *Construction and Building Materials*, **246**, Article 118421. https://doi.org/10.1016/j.conbuildmat.2020.118421

[4] Calderon, C., Cantu, C. and Chuhan-Pole, P. (2018) Infrastructure Development in Sub-Saharan Africa: A Scorecard. World Bank.

[5] Abdulazeez, A. (2025) Sand Dynamics and Utilization in the Geographical Context of Fluvial Geomorphology and Watershed Hydrology. *Journal of Geography, Environment and Earth Science International*, **29**, 46-61. https://doi.org/10.9734/jgeesi/2025/v29i6905

[6] Mathias Kondolf, G. (1994) Geomorphic and Environmental Effects of Instream Gravel Mining. *Landscape and Urban Planning*, **28**, 225-243. https://doi.org/10.1016/0169-2046(94)90010-8

[7] Grim, R.E. (1962) Clay Mineralogy. *Science*, **135**, 890-898. https://doi.org/10.1126/science.135.3507.890

[8] Abdullah, A.H. and Mohammed, S.D. (2023) Effect of Lightweight Expanded Clay Aggregate as Partial Replacement of Coarse Aggregate on the Mechanical Properties

of Fire-Exposed Concrete. *Journal of the Mechanical Behavior of Materials*, **32**, Article No. 20220299. https://doi.org/10.1515/jmbm-2022-0299

[9] Wei, Y., Chen, Z., Yio, M., Cheeseman, C., Wang, H. and Poon, C.S. (2025) Advanced Moisture Control in Porous Aggregates for Improved Lightweight High-Performance Concrete. *Cement and Concrete Composites*, **155**, Article 105826. https://doi.org/10.1016/j.cemconcomp.2024.105826

[10] Pongsopha, P., Sukontasukkul, P., Zhang, H. and Limkatanyu, S. (2022) Thermal and Acoustic Properties of Sustainable Structural Lightweight Aggregate Rubberized Concrete. *Results in Engineering*, **13**, Article 100333. https://doi.org/10.1016/j.rineng.2022.100333

[11] Nadesan, M.S. and Dinakar, P. (2017) Structural Concrete Using Sintered Flyash Lightweight Aggregate: A Review. *Construction and Building Materials*, **154**, 928-944. https://doi.org/10.1016/j.conbuildmat.2017.08.005

[12] Riley, C.M. (1951) Relation of Chemical Properties to the Bloating of Clays. *Journal of the American Ceramic Society*, **34**, 121-128. https://doi.org/10.1111/j.1151-2916.1951.tb11619.x

[13] Aboudi Mana, S.C., Hanafiah, M.M. and Chowdhury, A.J.K. (2017) Environmental Characteristics of Clay and Clay-Based Minerals. *Geology, Ecology, and Landscapes*, **1**, 155-161. https://doi.org/10.1080/24749508.2017.1361128

[14] Gliozzo, E. (2020) Ceramic Technology. How to Reconstruct the Firing Process. *Archaeological and Anthropological Sciences*, **12**, Article No. 260. https://doi.org/10.1007/s12520-020-01133-y

[15] da Silva Neto, J.A., dos Anjos, M.A.S., Dutra, R.P.S., Mendonça de Souza, M. and Pederneiras, C.M. (2025) Optimization via Taguchi of Artificial Lightweight Aggregates Obtained from Kaolinite Clay and Ceramic Waste: Development and Industrial Applications. *Buildings*, **15**, Article 2003. https://doi.org/10.3390/buildings15122003

[16] Decleer, J. and Viaene, W. (1993) Rupelian Boom Clay as Raw Material for Expanded Clay Manufacturing. *Applied Clay Science*, **8**, 111-128. https://doi.org/10.1016/0169-1317(93)90032-v

[17] Liao, Y.-C. and Huang, C.-Y. (2011) Effects of Cao Addition on Lightweight Aggregates Produced from Water Reservoir Sediment. *Construction and Building Materials*, **25**, 2997-3002. https://doi.org/10.1016/j.conbuildmat.2010.12.034

[18] Wie, Y.M., Lee, K.G. and Lee, K.H. (2020) Chemical Design of Lightweight Aggregate to Prevent Adhesion at Bloating Activation Temperature. *Journal of Asian Ceramic Societies*, **8**, 245-254. https://doi.org/10.1080/21870764.2020.1725259

[19] Hammond, G.P. (2018) System Characterisation of Carbon Capture and Storage (CCS) Systems. In: Clair, G., Patricia, T., Sarah, M., Naomi, V. and Temitope, F., Eds., *Biomass Energy with Carbon Capture and Storage* (*BECCS*): *Unlocking Negative Emissions*, John Wiley & Sons, Ltd, 129-162. https://doi.org/10.1002/9781119237716.ch7

[20] Schandl, H., Fischer-Kowalski, M., West, J., Giljum, S., Dittrich, M., Eisenmenger, N., *et al.* (2017) Global Material Flows and Resource Productivity: Forty Years of Evidence. *Journal of Industrial Ecology*, **22**, 827-838. https://doi.org/10.1111/jiec.12626

[21] Uceda-Rodríguez, M., Moreno-Maroto, J.M., Cobo-Ceacero, C.J., López-García, A.B., Cotes-Palomino, T. and Martínez-García, C. (2022) Comparative Life Cycle Assessment of Lightweight Aggregates Made from Waste—Applying the Circular Economy. *Applied Sciences*, **12**, Article 1917. https://doi.org/10.3390/app12041917

[22] Djongyang, N. (2022) Climate Change and Some Adaptation Measures in the Su-

dano-Sahelian Zone of Cameroon. *E3S Web of Conferences*, **354**, Article 01004. https://doi.org/10.1051/e3sconf/202235401004

[23] Nkiaka, E., Nawaz, N.R. and Lovett, J.C. (2017) Analysis of Rainfall Variability in the Logone Catchment, Lake Chad Basin. *International Journal of Climatology*, **37**, 3553-3564. https://doi.org/10.1002/joc.4936

[24] Mkoumbe, E., Estelle Eric, F.T.M., Albert, E.Y., Philippe, N.N. and Tabod, T.C. (2019) Depositional and Structural Styles in the Logone Birni Basin (LBB), Northern Cameroon, from 3D Potential Field Modeling: Preliminary Results. *Open Journal of Geology*, **9**, 226-244. https://doi.org/10.4236/ojg.2019.94016

[25] Westra, T. and De Wulf, R.R. (2009) Modelling Yearly Flooding Extent of the Waza-Logone Floodplain in Northern Cameroon Based on MODIS and Rainfall Data. *International Journal of Remote Sensing*, **30**, 5527-5548. https://doi.org/10.1080/01431160802672872

[26] Sababa, E., Ekoa Bessa, A.Z., Aye, B.A., Loubahndem, A.S. and Welba, M. (2023) Alluvial Sediments in Bol Area (Lake Chad Basin): Implications for Source Area-Weathering and Tectonic Settings. *Journal of Sedimentary Environments*, **8**, 563-586. https://doi.org/10.1007/s43217-023-00148-4

[27] Loule, J. and Pospisil, L. (2013) Geophysical Evidence of Cretaceous Volcanics in Logone Birni Basin (Northern Cameroon), Central Africa, and Consequences for the West and Central African Rift System. *Tectonophysics*, **583**, 88-100. https://doi.org/10.1016/j.tecto.2012.10.021

[28] Bate, S.C.C. (1979) Guide for Structural Lightweight Aggregate Concrete: Report of ACI Committee 213. *International Journal of Cement Composites and Lightweight Concrete*, **1**, 5-6. https://doi.org/10.1016/0262-5075(79)90004-6

[29] Tsozué, D., Nzeukou, A.N., Kagonbé, B.P., Madi, A.B., Mache, J.R., Bitom, D.L., *et al.* (2022) Genesis and Assessment of Clay Materials Suitability for Earthenware Production in Northern Cameroon. *Arabian Journal of Geosciences*, **15**, Article No. 1376. https://doi.org/10.1007/s12517-022-10603-7

[30] Andrade, F.A., Al-Qureshi, H.A. and Hotza, D. (2011) Measuring the Plasticity of Clays: A Review. *Applied Clay Science*, **51**, 1-7. https://doi.org/10.1016/j.clay.2010.10.028

[31] Holtz, R. and Kovacs, W.D. (1981) An Introduction to Geotechnical Engineering. Prentice-Hall, 747.

[32] Ntouala, R.F.D., Ndome-Priso, E., Nanga, M.T.B., Mutlen, J.A., Ze, A.N., Onana, V.L., *et al.* (2023) Mineralogy, Geochemistry, and Geotechnical Characterization of Lateritic and Alluvial Clay Deposits from Batouri, East Cameroon. *Arabian Journal of Geosciences*, **16**, Article No. 355. https://doi.org/10.1007/s12517-023-11451-9

[33] Zhu, Z., Zhou, Y., Li, X., Liu, L., Lu, Y. and Ren, T. (2025) Measuring Soil Particle Density Using Water Pycnometer: Influencing Factors, Errors, and Correction. *Soil Science Society of America Journal*, **89**, e70073. https://doi.org/10.1002/saj2.70073

[34] Wang, Y., He, Y., Zhan, J. and Li, Z. (2022) Identification of Soil Particle Size Distribution in Different Sedimentary Environments at River Basin Scale by Fractal Dimension. *Scientific Reports*, **12**, Article No. 10960. https://doi.org/10.1038/s41598-022-15141-6

[35] Khallah, Y.I., Lamido, A.K., Bala Muhammad, and Musa, A.S. (2025) Spatial and Geo-Statistical Analysis of Variability of the Soil Particle Size Distribution in River Wudil Floodplain, Kano State, Nigeria. *Sahel Journal of Life Sciences FUDMA*, **3**, 228-238. https://doi.org/10.33003/sajols-2025-030222-28

[36] Guan, X., Wang, J., Liu, G., Xiao, M., Ding, Y. and Chen, J. (2023) Grain Size Char-

acteristics of Surface Sediment in the Jilantai Salt Lake Protection System after Long-Term Wind-Sand Activities. *Land Degradation & Development*, **35**, 321-333. https://doi.org/10.1002/ldr.4918

[37] Temga, J.P., Mache, J.R., Madi, A.B., Nguetnkam, J.P. and Bitom, D.L. (2019) Ceramics Applications of Clay in Lake Chad Basin, Central Africa. *Applied Clay Science*, **171**, 118-132. https://doi.org/10.1016/j.clay.2019.02.003

[38] Wen, D., Wang, J., Ding, J. and Zhang, Z. (2025) Distribution Characteristics and Relationship between Soil Salinity and Soil Particle Size in Ebinur Lake Wetland, Xinjiang. *Land*, **14**, Article 297.

[39] Li, H., Meng, Z., Dang, X., Qi, S. and Bao, S. (2022) Grain Size Characteristics from Dry Playa Chagan Nur in Northern China. *Polish Journal of Environmental Studies*, **32**, 113-124. https://doi.org/10.15244/pjoes/153022

[40] Zhao, C., Shao, M., Jia, X. and Zhang, C. (2016) Particle Size Distribution of Soils (0 - 500 cm) in the Loess Plateau, China. *Geoderma Regional*, **7**, 251-258. https://doi.org/10.1016/j.geodrs.2016.05.003

[41] Sowiński, P., Smólczyński, S., Orzechowski, M., Kalisz, B. and Bieniek, A. (2023) Effect of Soil Agricultural Use on Particle-Size Distribution in Young Glacial Landscape Slopes. *Agriculture*, **13**, Article 584. https://doi.org/10.3390/agriculture13030584

[42] Kagonbé, B.P., Tsozué, D., Nzeukou, A.N. and Ngos III, S. (2021) Mineralogical, Geochemical and Physico-Chemical Characterization of Clay Raw Materials from Three Clay Deposits in Northern Cameroon. *Journal of Geoscience and Environment Protection*, **9**, 86-99. https://doi.org/10.4236/gep.2021.96005

[43] Nzeukou Nzeugang, A., Tsozué, D., Kagonbé Pagna, B., Balo Madi, A., Fankam Deumeni, A., Ngos, S., *et al.* (2021) Clayey Soils from Boulgou (North Cameroon): Geotechnical, Mineralogical, Chemical Characteristics and Properties of Their Fired Products. *SN Applied Sciences*, **3**, Article No. 551. https://doi.org/10.1007/s42452-021-04541-4

[44] Moctar, I.B., Yannick, T.L., Albertine, A.S., Mache, J.R. and Mominou, N. (2023) Physico-Chemical, Mineralogical Characterization, and Ceramic Properties of Clay Materials from South Mindif (Far North, Cameroon). *JMST Advances*, **5**, 13-26. https://doi.org/10.1007/s42791-023-00047-9

[45] Yanné, E., Oumarou, A.A., Nde, B.D. and Danwé, R. (2018) Physico-Chemical and Mineralogical Characterization of Two Clay Materials of the Far North Region of Cameroon (Makabaye, Maroua). *Advances in Materials Physics and Chemistry*, **8**, 378-386. https://doi.org/10.4236/ampc.2018.89025

[46] Noubissie, N.M.M., Nzeukou, A.N., Tsozué, D., *et al.* (2016) Origin, Mineralogical Distribution, and Industrial Suitability of Clay-Rich Soils in the Semi-Arid Zone of Cameroon. *Geosystems Geoenvironment*, **5**, Article 100528. https://doi.org/10.1016/j.geogeo.2026.100528

[47] Bakaiyang, L., Duc, M., Boussafir, Y., Szymkiewicz, F. and Madjadoumbaye, J. (2024) Swelling-Shrinkage Properties of Compacted Karal Soils from North and Far North Cameroon: A Physicochemical and Geotechnical Approach. *European Journal of Environmental and Civil Engineering*, **28**, 2345-2365. https://doi.org/10.1080/19648189.2024.2314114

[48] BiLGiÇ, C. and Bilgiç, Ş. (2019) Fourier dönüşümlü kizilötesi (Ftir) spektroskopisinin killerin analizlerinde kullanilmasi. *Nevşehir Bilim ve Teknoloji Dergisi*, **8**, 37-46.

[49] Madejová, J. and Komadel, P. (2001) Baseline Studies of the Clay Minerals Society Source Clays: Infrared Methods. *Clays and Clay Minerals*, **49**, 410-432. https://doi.org/10.1346/ccmn.2001.0490508

[50] Kloprogge, J. (2018) The Kaolin Group: Hydroxyl Groups. In: (Theo) Kloprogge, J., Ed., *Spectroscopic Methods in the Study of Kaolin Minerals and Their Modifications*, Springer International Publishing, 41-96. https://doi.org/10.1007/978-3-030-02373-7_3

[51] Jozanikohan, G. and Abarghooei, M.N. (2022) The Fourier Transform Infrared Spectroscopy (FTIR) Analysis for the Clay Mineralogy Studies in a Clastic Reservoir. *Journal of Petroleum Exploration and Production Technology*, **12**, 2093-2106. https://doi.org/10.1007/s13202-021-01449-y

[52] Madjihingam, N., Pagore, D., Mache, J.R., Warabi, B., Kagonbe, B.P. and Kouotou, P.M. (2024) Clay Materials for Ceramics Application from N'djamena in the Chad Republic: Mineralogical, Physicochemical and Microstructural Characterization. *Journal of Materials Science and Chemical Engineering*, **12**, 31-48. https://doi.org/10.4236/msce.2024.122003

[53] Sababa, E., Bessa, A.Z.E., Beyanu, A.A., Loubahndem, A.S.-B. and Welba, M. (2023) Morphological, Mineralogical and Geochemical Features of Alluvial Sediments in Bol area (Lake Chad Basin): Implications for Source Area-Weathering and Tectonic Settings. Research Square.

[54] Djomgoue, P. and Njopwouo, D. (2013) FT-IR Spectroscopy Applied for Surface Clays Characterization. *Journal of Surface Engineered Materials and Advanced Technology*, **3**, 275-282. https://doi.org/10.4236/jsemat.2013.34037

[55] Bernhardt, M., Tellesbø, H., Justnes, H. and Wiik, K. (2013) Mechanical Properties of Lightweight Aggregates. *Journal of the European Ceramic Society*, **33**, 2731-2743. https://doi.org/10.1016/j.jeurceramsoc.2013.05.013

[56] Dondi, M., Cappelletti, P., D'Amore, M., de Gennaro, R., Graziano, S.F., Langella, A., *et al.* (2016) Lightweight Aggregates from Waste Materials: Reappraisal of Expansion Behavior and Prediction Schemes for Bloating. *Construction and Building Materials*, **127**, 394-409. https://doi.org/10.1016/j.conbuildmat.2016.09.111

[57] Yeşilbaş, M., Holmboe, M. and Boily, J. (2018) Cohesive Vibrational and Structural Depiction of Intercalated Water in Montmorillonite. *ACS Earth and Space Chemistry*, **2**, 38-47. https://doi.org/10.1021/acsearthspacechem.7b00103

[58] Frost, R.L., Kristof, J., Paroz, G.N. and Kloprogge, J.T. (1998) Role of Water in the Intercalation of Kaolinite with Hydrazine. *Journal of Colloid and Interface Science*, **208**, 216-225. https://doi.org/10.1006/jcis.1998.5780

[59] Chen, L., He, X., Liu, H., Qian, L. and Kim, S.H. (2018) Water Adsorption on Hydrophilic and Hydrophobic Surfaces of Silicon. *The Journal of Physical Chemistry C*, **122**, 11385-11391. https://doi.org/10.1021/acs.jpcc.8b01821

[60] Peng, L., Qisui, W., Xi, L. and Chaocan, Z. (2009) Investigation of the States of Water and OH Groups on the Surface of Silica. *Colloids and Surfaces A*: *Physicochemical and Engineering Aspects*, **334**, 112-115. https://doi.org/10.1016/j.colsurfa.2008.10.028

[61] D'Elia, A., Pinto, D., Eramo, G., Laviano, R., Palomo, A. and Fernández-Jiménez, A. (2020) Effect of Alkali Concentration on the Activation of Carbonate-High Illite Clay. *Applied Sciences*, **10**, Article 2203. https://doi.org/10.3390/app10072203

[62] Hasanin, T.H.A., Alsahli, S.A., Altaleb, H.A., Alshammari, B.H. and Tantawy, M.A. (2025) Hydration Characteristics of Cement Blended with Thermally Reactivated Recycled Concrete Demolition Waste. *Scientific Reports*, **16**, Article No. 1499. https://doi.org/10.1038/s41598-025-31881-7

[63] Pisciella, P. and Pelino, M. (2005) FTIR Spectroscopy Investigation of the Crystallisation Process in an Iron Rich Glass. *Journal of the European Ceramic Society*, **25**,

1855-1861. https://doi.org/10.1016/j.jeurceramsoc.2004.06.012

[64] Liu, H., Kaya, H., Lin, Y., Ogrinc, A. and Kim, S.H. (2022) Vibrational Spectroscopy Analysis of Silica and Silicate Glass Networks. *Journal of the American Ceramic Society*, **105**, 2355-2384. https://doi.org/10.1111/jace.18206

[65] Peternella, W.S. and Costa, A.C.S.D. (2021) Evaluation of a Toposequence of Soils Derived from Basalt by Fourier Transform Infrared Spectroscopy. *OALib*, **8**, 1-17. https://doi.org/10.4236/oalib.1107867

[66] Moussa, A., Novello, A., Lebatard, A., Decarreau, A., Fontaine, C., Barboni, D., *et al.* (2016) Lake Chad Sedimentation and Environments during the Late Miocene and Pliocene: New Evidence from Mineralogy and Chemistry of the Bol Core Sediments. *Journal of African Earth Sciences*, **118**, 192-204. https://doi.org/10.1016/j.jafrearsci.2016.02.023

[67] Comin, A.B., Zaccaron, A., de Souza Nandi, V., Inocente, J.M., Muller, T.G., Dal Bó, A.G., *et al.* (2021) Measurement of Apparent Sintering Activation Energy for Densification of Clays. *Clay Minerals*, **56**, 299-305. https://doi.org/10.1180/clm.2022.11

[68] Bebbata, W., Djoda, F.P., Ndjolba, M., Kagonbé, B.P. and Danwé, R. (2024) Geochemistry and Microstructure of Construction Materials from the Eastern Districts of N'Djamena Chad with a View to Their Stabilization in the Building and Pottery. *Materials Sciences and Applications*, **15**, 431-449. https://doi.org/10.4236/msa.2024.1510029

[69] Kusiorowski, R., Zaremba, T., Piotrowski, J. and Podwórny, J. (2015) Utilisation of Cement-Asbestos Wastes by Thermal Treatment and the Potential Possibility Use of Obtained Product for the Clinker Bricks Manufacture. *Journal of Materials Science*, **50**, 6757-6767. https://doi.org/10.1007/s10853-015-9231-6

[70] Ghizdavet, Z.D., Simion, C.A., Ficai, A., Oprea, O., Fierascu, R.C., Marin, M.L., *et al.* (2025) Investigations on an Ancient Mortar from Ulpia Traiana Sarmizegetusa Archaeological Site, Romania. *Applied Sciences*, **15**, Article 5780. https://doi.org/10.3390/app15105780

[71] Deon, F., van Ruitenbeek, F., van der Werff, H., van der Meijde, M. and Marcatelli, C. (2022) Detection of Interlayered Illite/Smectite Clay Minerals with XRD, SEM Analyses and Reflectance Spectroscopy. *Sensors*, **22**, Article 3602. https://doi.org/10.3390/s22093602

[72] Audu, J. and Osuji, S. (2025) Evaluation of Makurdi Clays for Sustainable Brick Production and Their Pozzolanic Potential. *Discover Civil Engineering*, **2**, Article No. 175. https://doi.org/10.1007/s44290-025-00338-1

[73] Goltsman, B.M. and Yatsenko, E.A. (2024) Modern Fluxing Materials and Analysis of Their Impact on Silicate Structures: A Review. *Open Ceramics*, **17**, Article 100540. https://doi.org/10.1016/j.oceram.2024.100540

[74] Shao, Y., Hu, G., Liu, Z., Xu, X., Zhang, M., Ding, C., *et al.* (2022) Determination of Band Structure of Naturally Occurring Goethite with Al Substitution: A Case Study of Zhushan Iron Zone. *Materials*, **15**, Article 1465. https://doi.org/10.3390/ma15041465

[75] Smoleń, J., Fross, K., Groń, K., Orzechowska, K., Stępień, K., Junak, G., *et al.* (2024) Utilization of Lightweight Ceramic Aggregates Based on Waste Materials in the Production of Lightweight Polymer Concrete as a Component of Sustainable Architecture. *Scientific Reports*, **14**, Article No. 29384. https://doi.org/10.1038/s41598-024-81290-5

[76] Viana Rodrigues, A. and Roca Bragança, S. (2023) An Evaluation of the Increased Expansion of Clay Aggregates Fired at 1300˚C to Maximize Lightness for Non-Struc-

tural Concrete. *Boletín de la Sociedad Española de Cerámica y Vidrio*, **62**, 56-65. https://doi.org/10.1016/j.bsecv.2021.11.003

[77] Ansyori, A., Prasetyo, A., Ojahan Rajagukguk, T., Hartawan, B. and Hendronursito, Y. (2025) Characterization of the Properties of South Lampung Clay as Lightweight Expanded Clay Aggregate. *Journal of Science and Technology*, **17**, 33-40. https://doi.org/10.30880/jst.2025.17.01.004

[78] Almajeed, E.A. and Turki, S.K. (2018) Synthesis of Expanded Clay Aggregate Pellets by Using Local Raw Materials. *Journal of University of Babylon for Engineering Sciences*, **26**, 345-353. https://doi.org/10.29196/jub.v26i4.812

[79] Cultrone, G., Sebastián, E., Elert, K., de la Torre, M.J., Cazalla, O. and Rodriguez–Navarro, C. (2004) Influence of Mineralogy and Firing Temperature on the Porosity of Bricks. *Journal of the European Ceramic Society*, **24**, 547-564. https://doi.org/10.1016/s0955-2219(03)00249-8

[80] Ayati, B., Ferrándiz-Mas, V., Newport, D. and Cheeseman, C. (2018) Use of Clay in the Manufacture of Lightweight Aggregate. *Construction and Building Materials*, **162**, 124-131. https://doi.org/10.1016/j.conbuildmat.2017.12.018

[81] Rodrigues, A.V. and Bragança, S.R. (2023) Technological Properties of a Self-Bloating Clay and Expanded-Clay Aggregate for the Production of Lightweight Concrete. *Cerâmica*, **69**, 6-16. https://doi.org/10.1590/0366-69132023693893308

[82] Murugesan, P., Partheeban, P., Manimuthu, S., Jegadeesan, V. and Christopher, C.G. (2023) Multi-Criteria Decision Analysis for Optimum Selection of Different Construction Bricks. *Journal of Building Engineering*, **71**, Article 106440. https://doi.org/10.1016/j.jobe.2023.106440

[83] Serpell, R. and Zwicky, D. (2021) Low-Energy Lightweight Aggregates by Cold Bonding of Biomass Wastes: Effects of Raw Material Proportion Adjustments on Product Properties. *SSRN Electronic Journal*, 32 p. https://doi.org/10.2139/ssrn.3985209

[84] Moreno-Maroto, J.M., Uceda-Rodríguez, M., Cobo-Ceacero, C.J., Cotes-Palomino, T., Martínez-García, C. and Alonso-Azcárate, J. (2020) Studying the Feasibility of a Selection of Southern European Ceramic Clays for the Production of Lightweight Aggregates. *Construction and Building Materials*, **237**, Article 117583. https://doi.org/10.1016/j.conbuildmat.2019.117583

[85] Fakhfakh, E., Hajjaji, W., Medhioub, M., Rocha, F., Lopezgalindo, A., Setti, M., *et al.* (2007) Effects of Sand Addition on Production of Lightweight Aggregates from Tunisian Smectite-Rich Clayey Rocks. *Applied Clay Science*, **35**, 228-237. https://doi.org/10.1016/j.clay.2006.09.006

[86] Escalera, E., Antti, M.L. and Odén, M. (2012) Thermal Treatment and Phase Formation in Kaolinite and Illite Based Clays from Tropical Regions of Bolivia. *IOP Conference Series: Materials Science and Engineering*, **31**, Article 012017. https://doi.org/10.1088/1757-899x/31/1/012017

[87] Elgamouz, A., Tijani, N., Shehadi, I., Hasan, K. and Al-Farooq Kawam, M. (2019) Characterization of the Firing Behaviour of an Illite-Kaolinite Clay Mineral and Its Potential Use as Membrane Support. *Heliyon*, **5**, e02281. https://doi.org/10.1016/j.heliyon.2019.e02281

[88] Jordán, M.M., Meseguer, S., Pardo, F. and Montero, M.A. (2020) High-Temperature Mineral Formation after Firing Clay Materials Associated with Mined Coal in Teruel (Spain). *Applied Sciences*, **10**, Article 3114. https://doi.org/10.3390/app10093114

[89] Wang, S., Gainey, L., Baxter, D., Wang, X., Mackinnon, I.D.R. and Xi, Y. (2021) Thermal Behaviours of Clay Mixtures during Brick Firing: A Combined Study of *In-Situ* XRD, TGA and Thermal Dilatometry. *Construction and Building Materials*, **299**, Ar-

ticle 124319. https://doi.org/10.1016/j.conbuildmat.2021.124319

[90] Húlan, T. and Štubňa, I. (2020) Young's Modulus of Kaolinite-Illite Mixtures during Firing. *Applied Clay Science*, **190**, Article 105584. https://doi.org/10.1016/j.clay.2020.105584

[91] Kaljuvee, T., Štubňa, I., Húlan, T., Uibu, M., Einard, M., Traksmaa, R., *et al.* (2021) Thermal Behavior of Ceramic Bodies Based on Estonian Clay from the Arumetsa Deposit with Oil Shale Ash and Clinker Dust Additives. *Processes*, **10**, Article 46. https://doi.org/10.3390/pr10010046

[92] Martínez, J.D., Betancourt-Parra, S., Carvajal-Marín, I. and Betancur-Vélez, M. (2018) Ceramic Light-Weight Aggregates Production from Petrochemical Wastes and Carbonates ($NaHCO_3$ and $CaCO_3$) as Expansion Agents. *Construction and Building Materials*, **180**, 124-133. https://doi.org/10.1016/j.conbuildmat.2018.05.281

[93] Abdel-Kader, N., EL-Raoof, F.A., Sharaf-Eldin, A., Elmasry, A., Yahya, A., Zacher, G., *et al.* (2024) Clays to Lightweight Aggregates: Thermochemical Modeling and Industrial Validation. *Construction and Building Materials*, **432**, Article 136580. https://doi.org/10.1016/j.conbuildmat.2024.136580

[94] Moreno-Maroto, J.M., Cobo-Ceacero, C.J., Martínez-Rodríguez, A.M., Conde-Sánchez, A., González-Corrochano, B., Alonso-Azcárate, J., *et al.* (2023) Study of the Synergistic Impact of Fe_3O_4, Na_2CO_3 and Organic C on Kaolin-Based Lightweight Aggregates by a DOE (Mixture Experiments) Approach. *Construction and Building Materials*, **403**, Article 133152. https://doi.org/10.1016/j.conbuildmat.2023.133152

[95] Kieufack, G., Bomeni, I.Y., Ngapgue, F., Tchamba, A.B., Mbog, M.B., Kouonang, S.T., *et al.* (2021) Potential Use of Alluvial Clays from Monoun in Ceramics by Adding Feldspar from Batie (West-Cameroon) as a Fluxing Agent. *SN Applied Sciences*, **3**, Article No. 856. https://doi.org/10.1007/s42452-021-04837-5

[96] Chen, Y.H. (2013) Thermal Properties of Nanocrystalline Goethite, Magnetite, and Maghemite. *Journal of Alloys and Compounds*, **553**, 194-198. https://doi.org/10.1016/j.jallcom.2012.11.102

[97] Peys, A., Van De Sande, J., Teck, P. and Snellings, R. (2021) A Metallurgical Approach toward Bloating of Canal-Dredging Sediments. *Journal of Sustainable Metallurgy*, **7**, 1671-1685. https://doi.org/10.1007/s40831-021-00441-4